Molecular and Electronic Structures of Bis[1,4-bis(trimethylsilyl)cyclooctatetraene] Sandwich Complexes of Titanium and Zirconium†

F. Geoffrey N. Cloke,[a] Jennifer C. Green,[c] Peter B. Hitchcock,[a] Stephen C. P. Joseph,[a] Philip Mountford,[b] Nikolas Kaltsoyannis[c] and Andrew McCamley[d]

[a] *School of Chemistry and Molecular Sciences, University of Sussex, Brighton BN1 9QJ, UK*
[b] *Department of Chemistry, University of Nottingham, Nottingham NG7 2RD, UK*
[c] *Department of Inorganic Chemistry, University of Oxford, Oxford OX1 3QR, UK*
[d] *Department of Chemistry, University of Warwick, Coventry CV4 7AL, UK*

The reaction between 2 equivalents of $[Li_2\{C_8H_6(SiMe_3)_2\}]$ and $[MCl_4(thf)_2]$ (M = Ti or Zr) in tetrahydrofuran (thf) afforded the sandwich complexes $[M\{C_8H_6(SiMe_3)_2\}_2]$. X-Ray studies showed that the zirconium compound adopts a structure in which one ring is bound in an η^8 fashion whilst the other adopts a novel η^3 co-ordination mode. This unusual bonding situation has been studied using extended-Hückel molecular-orbital calculations and photoelectron spectroscopy. In contrast, the titanium compound adopts a solid-state structure in which one ring is η^8 bound and the other is less readily classified, being intermediate between the η^3 structure found for Zr and the η^4 structure found in $[Ti(C_8H_8)_2]$. Variable-temperature solution NMR studies on $[M\{C_8H_6(SiMe_3)_2\}_2]$ showed that the two rings remain indistinguishable even at 193 K for M = Zr, whereas for M = Ti the two rings only become equivalent on the NMR time-scale above 328 K.

We have recently described the synthesis and utility of 1,4-bis(trimethylsilyl)cyclooctatetraene $[C_8H_6(SiMe_3)_2]$ as a ligand for organo-f-element chemistry, in particular.[1,2] We were also interested to explore the potential of this sterically demanding compound in early transition-metal chemistry, and herein report the syntheses and structures of the sandwich compounds $[M\{C_8H_6(SiMe_3)_2\}_2]$, M = Ti or Zr, and discuss the unusual solid-state structure of the zirconium complex. During the course of this work the synthesis of the latter was independently reported by Floriani and co-workers,[3] although the crystal structure was not determined.

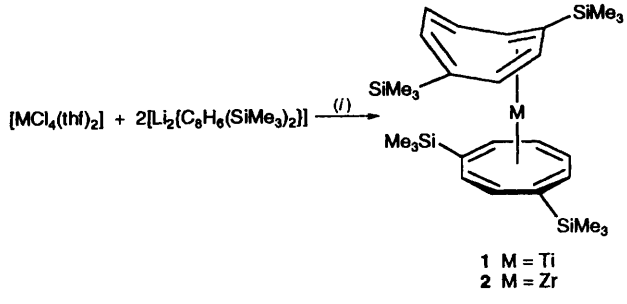

Scheme 1 (*i*) thf, 273 K

Results and Discussion

Bis[1,4-*bis*(*trimethylsilyl*)*cyclooctatetraene*]*titanium*.—Deep red $[Ti\{C_8H_6(SiMe_3)_2\}_2]$ **1** was prepared by the simple metathesis of $[TiCl_4(thf)_2]$ with 2 equivalents of $[Li_2\{C_8H_6(SiMe_3)_2\}]$ in tetrahydrofuran (thf), and purified by sublimation (see Scheme 1).

Solution NMR data (see Experimental section) measured at 295 K indicate that the rings in **1** adopt η^8 and η^4 bonding modes, in similar fashion to those in the unsubstituted analogue $[Ti(C_8H_8)_2]$.[4] The ^1H NMR spectrum shows separate resonances for both the η^8- and η^4-bound ring protons, which give AA'BB'X_2 multiplets. The ^{13}C NMR spectrum confirms the solution structure of the molecule: eight resonances are observed downfield between δ 90 and 121, associated with the ring carbons, while two resonances are seen at higher field, attributable to the $SiMe_3$ substituents of the two rings. The ^{29}Si NMR spectrum also shows the two resonances anticipated at room temperature.

These data are consistent with a structure in which the η^4 ring undergoes a rapid haptotropic shift around the titanium centre, while the other ring remains constantly η^8. That the ^{13}C NMR resonances for the ring carbons are grouped closely together around δ 110 indicates that the titanium migrates over all possible centres, and does not simply shuffle between two η^4 sites, which would also lead to the observed equivalence of the two $SiMe_3$ groups of the η^4 ring [the ^{13}C resonances for the ring carbons in free $C_8H_6(SiMe_3)_2$ are in the range δ 129–149,[2] whereas those for the η^4 ring in **1** all occur in the range δ 100–121, indicating that all carbons must spend some time co-ordinated to titanium].

At elevated temperatures, however, the ring and $SiMe_3$ resonances in the ^1H NMR spectrum of compound **1** were observed to broaden and move closer together until at *ca.* 304 K coalescence was observed. By 328 K, one singlet (although somewhat broad) was observed for all $SiMe_3$ groups, indicating that the rings are rapidly interconverting *via* a mechanism which has not been established. These variable-temperature studies afford a value of $\Delta G^{\ddagger} = 68 \pm 1$ kJ mol^{-1} for the ring interconversion, comparable to a value of 69 ± 1 kJ mol^{-1} for $[Ti(C_8H_8)_2]$.[4]

The molecular structure of compound **1** is shown in Fig. 1; selected bond parameters and atomic coordinates are collected in Tables 1 and 2 respectively. The structure shows the expected η^8, η^4 co-ordination of the two ligands, affording the molecule a

† *Supplementary data available*: see Instructions for Authors, *J. Chem. Soc., Dalton Trans.*, 1994, Issue 1, pp. xxiii–xxviii.
Non-SI unit employed: eV ≈ 1.6 × 10^{-19} J.

formal electron count of 16. While the planar η^8 ring shows no significant distortions within the carbon framework (average C–C bond distance 1.41 Å), the two carbon atoms bearing the $SiMe_3$ substituents are substantially further from the metal centre than the six remaining carbons [average Ti–C($SiMe_3$) distance 2.356, average Ti–C(H) bond distance 2.293 Å]. The molecular structure of $[Ti(C_8H_8)_2]$ shows no comparable distortions (average Ti–C *ca.* 2.32 Å).[5]

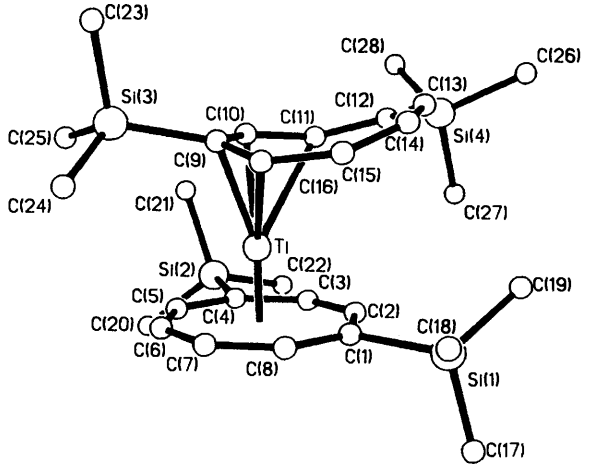

Fig. 1 Molecular structure of $[Ti\{C_8H_6(SiMe_3)_2\}_2]$

Table 1 Selected bond distances (Å) and angles (°) in $[Ti\{C_8H_6(SiMe_3)_2\}_2]$

Ti–C(9)	2.163(8)	C(16)–C(9)	1.414(16)
Ti–C(10)	2.229(10)	C(9)–C(10)	1.426(15)
Ti–C(11)	2.664(9)	C(10)–C(11)	1.414(13)
Ti–C(16)	2.354(10)	C–C for η^8 ring (av.)	1.403
Ti–C for η^8 ring (av.)	2.310		
C(10)–C(9)–C(16)	125.2(8)	C(9)–C(16)–C(15)	136.2(9)
C(11)–C(10)–C(9)	134.1(9)	C(12)–C(13)–C(14)	132.2(8)

Table 2 Fractional atomic coordinates ($\times 10^4$) for $[Ti\{C_8H_6(SiMe_3)_2\}_2]$

Atom	*x*	*y*	*z*
Ti	9 745.9(9)	6 101.0(11)	7 423.1
Si(1)	9 601(2)	8 810(2)	6 084(2)
Si(2)	8 702(2)	6 395(3)	9 387(3)
Si(3)	10 610(2)	3 288(2)	7 412(3)
Si(4)	12 158(2)	8 578(3)	8 575(3)
C(1)	9 247(7)	7 667(8)	6 742(6)
C(2)	9 348(6)	7 998(6)	7 457(6)
C(3)	9 129(7)	7 526(9)	8 121(5)
C(4)	8 749(7)	6 499(9)	8 396(6)
C(5)	8 442(7)	5 525(10)	8 046(7)
C(6)	8 348(6)	5 160(7)	7 348(7)
C(7)	8 542(7)	5 620(8)	6 670(6)
C(8)	8 902(6)	6 660(8)	6 437(6)
C(9)	10 870(5)	4 859(6)	7 369(6)
C(10)	10 996(6)	5 464(8)	8 018(6)
C(11)	11 268(6)	6 592(8)	8 190(5)
C(12)	11 876(6)	7 447(7)	7 911(6)
C(13)	12 260(6)	7 578(7)	7 249(6)
C(14)	12 028(7)	7 110(8)	6 593(6)
C(15)	11 419(7)	6 270(7)	6 364(6)
C(16)	10 928(7)	5 346(8)	6 684(6)
C(17)	8 559(8)	9 739(10)	5 994(7)
C(18)	9 880(9)	8 198(10)	5 201(6)
C(19)	10 621(8)	9 666(8)	6 410(7)
C(20)	7 571(12)	5 739(14)	9 641(8)
C(21)	9 670(9)	5 473(13)	9 716(7)
C(22)	8 793(14)	7 816(11)	9 816(7)
C(23)	11 718(6)	2 466(7)	7 315(9)
C(24)	9 811(7)	2 834(9)	6 697(7)
C(25)	10 074(10)	2 910(11)	8 283(7)
C(26)	13 119(8)	9 516(10)	8 272(8)
C(27)	11 143(8)	9 508(10)	8 746(8)
C(28)	12 529(10)	7 943(11)	9 424(7)

The second ring of compound **1** is puckered, with carbon atoms C(12)–C(15) clearly bent away from the metal centre. The Ti–C(11) bond distance of 2.664(9) Å is much longer than those to C(9), C(10) and C(16) [2.163(8), 2.229(10) and 2.354(10) Å, respectively]. While this is certainly shorter than the sum of the titanium and carbon van der Waals radii (*ca.* 4.20 Å), it remains an extremely long covalent bond. In contrast, the unsubstituted analogue $[Ti(C_8H_8)_2]$ contains a conventional, symmetrically bound η^4-C_8H_8 ring.[5] The distortions observed in **1**, described above, are attributable to the steric demands of the $SiMe_3$ substituents.

Bis[1,4-*bis*(*trimethylsilyl*)*cyclooctatetraene*]*zircononium*.—Purple $[Zr\{C_8H_6(SiMe_3)_2\}_2]$ **2** was prepared in a fashion analogous to that for compound **1**, essentially that reported by Floriani and co-workers[3] during the course of this work (see Scheme 1). In marked contrast to the solution behaviour of **1**, the spectra of **2** demonstrate that the two dynamic processes of ring whizzing and ring hapticity interconversion occur rapidly on the NMR time-scale. The ^1H NMR spectrum of **2** showed no changes down to 203 K.

The resonances associated with the hydrogen atoms of the rings of compound **2** are observed as complex multiplets at δ 6.32 and 5.85 characteristic of an AA'BB' system. The singlet at δ 6.35 is assigned to the two protons in the 2 and 3 positions on the rings, while the singlet observed at δ 0.35 corresponds to the protons of the $SiMe_3$ substituents. The ^{13}C-$\{^1H\}$ NMR spectrum shows five resonances which can be readily assigned to the rings. The INEPT (insensitive nuclei enhanced by polarisation transfer) spectrum shows only four resonances, allowing assignment of the quaternary carbons. The ^{29}Si-$\{^1H\}$ NMR spectrum shows only one resonance for all four silicon atoms in the molecule at any attainable temperatures, confirming that all environments are rapidly exchanging.

The molecular structure of compound **2** is shown in Fig. 2; selected bond parameters and atomic coordinates are collected in Tables 3 and 4 respectively. The η^8 ring, while planar, shows lengthened Zr–C($SiMe_3$) bond distances, in a similar fashion to that described for **1**. The puckered ring contains only three carbon atoms sufficiently close to the metal centre to be classed as bonded [C(1), C(2) and C(8)]. Atoms C(3) and C(7), 2.945(8) and 2.777(8) Å from the zirconium centre respectively, are too long to be considered as conventional covalent bonds. It would appear that the puckered ring adopts this η^3 co-ordination mode as a direct result of the steric congestion contributed by the $SiMe_3$ groups. The $SiMe_3$ group bonded to C(1) in the puckered ring is 'wedged' practically midway between the two ring substituents of the planar η^8 ring when viewed from below, suggesting that this staggered arrangement is a much preferred orientation. The η^8 ring itself, however, shows no unusual distortion from the plane as a result of this steric interaction.

The ^{29}Si solid-state cross polarisation magic angle spinning (CP MAS) NMR spectrum obtained for compound **2** shows four resonances, which confirms the four distinct environments for the silicon atoms.

Molecular-orbital calculations (see below) show that the energy difference between the structure as determined and the predicted structure in which the ligands bond in an η^8, η^4 arrangement is of the order of 0.1 eV, a value small enough to be considered negligible in the context of the above discussion.

Bonding in $[Zr\{C_8H_6(SiMe_3)_2\}_2]$.—(*i*) *Calculations on the model compounds* $[Zr(\eta^8\text{-}C_8H_8)(\eta^3\text{-}C_8H_8)]$ *and* $[Zr(\eta^8\text{-}C_8H_8)(\eta^4\text{-}C_8H_8)]$. The bonding in $[Zr\{\eta^8\text{-}C_8H_6(SiMe_3)_2\}\{\eta^3\text{-}C_8H_6(SiMe_3)_2\}]$ **2** was first investigated by performing

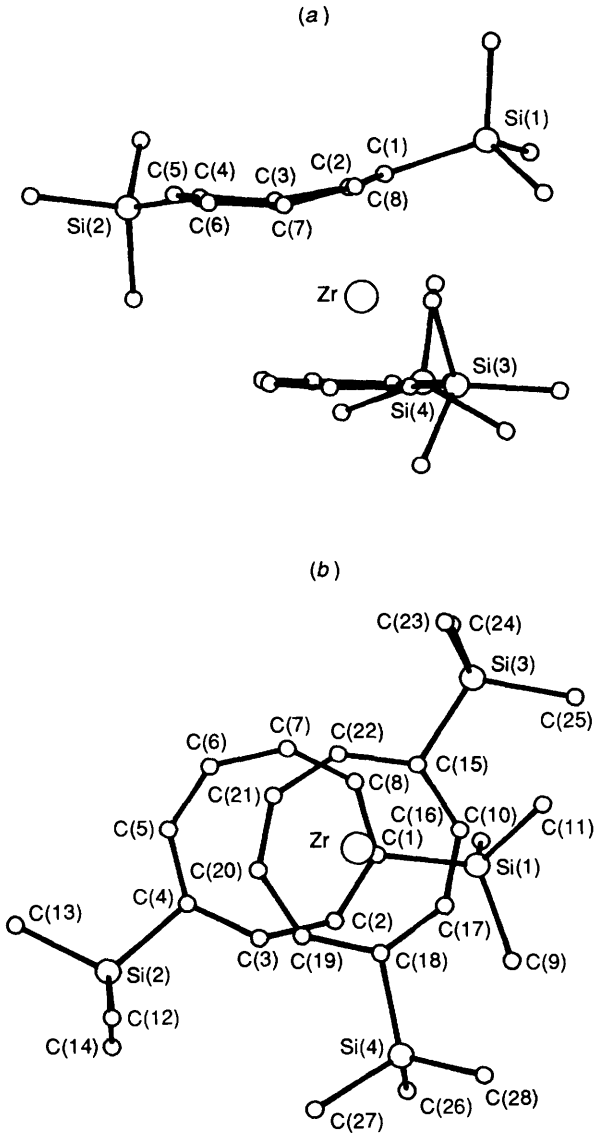

Fig. 2 Side (*a*) and bottom (*b*) views of the molecular structure of $[Zr\{C_8H_6(SiMe_3)_2\}_2]$

Table 3 Selected bond distances (Å) and angles in $[Zr\{C_8H_6(SiMe_3)_2\}_2]$

Zr–C(1)	2.300(8)	Zr–Centroid	1.587(1)
Zr–C(2)	2.440(8)	C(1)–C(2)	1.455(11)
Zr–C(3)	2.945(8)	C(2)–C(3)	1.401(11)
Zr–C(7)	2.777(8)	C(1)–C(8)	1.416(11)
Zr–C(8)	2.367(8)	C(8)–C(7)	1.401(12)
Zr–C in η^8 ring (av.)	2.436	C–C in η^8 ring (av.)	1.410
C(1)–C(8)–C(7)	134.6(8)	C(1)–C(2)–C(3)	135.3(7)
C(2)–C(1)–C(8)	127.9(7)		
Dihedral angle* in non-planar ring	161.4(6)		

* Between the planes defined by the atoms C(1), C(2), C(3), C(7), C(8) and C(3), C(4), C(5), C(6), C(7).

charge-iterative extended-Hückel molecular orbital (EHMO) calculations[6] on the model complex $[Zr(\eta^8\text{-}C_8H_8)(\eta^3\text{-}C_8H_8)]$. The atomic parameters used in all the calculations described below are listed in Table 5. The geometry of the model was based on that determined by X-ray analysis for **2** but idealised

Table 4 Fractional atomic coordinates ($\times 10^4$) for $[Zr\{C_8H_6(SiMe_3)_2\}_2]$

Atom	*x*	*y*	*z*
Zr	9 155.7(3)	4 114.0(3)	2 570.5(6)
Si(1)	9 664.9(9)	5 164.3(8)	1 836.8(19)
Si(2)	10 446.8(10)	3 353.7(9)	4 382.4(20)
Si(3)	8 207.6(9)	4 082.7(9)	594.1(19)
Si(4)	8 762.3(9)	4 563.4(9)	5 063.6(18)
C(1)	9 764(3)	4 548(3)	2 135(5)
C(2)	9 870(3)	4 445(3)	3 063(5)
C(3)	10 026(3)	4 063(3)	3 527(5)
C(4)	10 217(3)	3 632(3)	3 355(5)
C(5)	10 220(3)	3 383(3)	2 567(6)
C(6)	10 005(3)	3 429(3)	1 749(6)
C(7)	9 756(3)	3 773(3)	1 311(6)
C(8)	9 693(3)	4 239(3)	1 423(5)
C(9)	9 587(5)	5 519(4)	2 838(8)
C(10)	10 153(4)	5 384(4)	1 196(9)
C(11)	9 148(4)	5 223(3)	1 129(9)
C(12)	9 990(4)	3 236(4)	5 220(6)
C(13)	10 733(4)	2 810(4)	4 108(8)
C(14)	10 863(4)	3 717(5)	4 976(8)
C(15)	8 435(3)	3 992(3)	1 752(5)
C(16)	8 392(3)	4 364(3)	2 357(6)
C(17)	8 506(3)	4 455(3)	3 265(5)
C(18)	8 723(3)	4 235(3)	3 987(5)
C(19)	8 942(3)	3 802(3)	4 026(5)
C(20)	9 015(3)	3 441(3)	3 421(6)
C(21)	8 887(3)	3 339(2)	2 541(5)
C(22)	8 644(3)	3 565(3)	1 879(5)
C(23)	7 812(4)	3 609(4)	336(8)
C(24)	7 906(4)	4 629(4)	514(7)
C(25)	8 668(4)	4 078(4)	−248(7)
C(26)	9 297(8)	4 930(8)	5 079(14)
C(27)	8 891(12)	4 170(8)	6 035(13)
C(28)	8 286(8)	4 902(10)	5 208(16)
C(26a)	8 333(7)	4 305(7)	5 854(12)
C(27a)	8 551(11)	5 158(7)	4 877(15)
C(28a)	9 305(7)	4 538(10)	5 583(14)

so as to have C_s symmetry and with the $SiMe_3$ groups replaced by hydrogen atoms in order to simplify the analysis. The results of the EHMO calculations are presented in Fig. 3 in the form of an interaction diagram between a C_{8v} $Zr(\eta^8\text{-}C_8H_8)$ fragment (on the left) and a puckered C_8H_8 group possessing C_{2v} symmetry (on the right). The Zr–η^8-C_8H_8 ring centroid vector is taken as being coincident with the *z* axis in our choice of coordinate system. The pictorial representations of the wavefunctions alongside the fragment orbital energy levels in Fig. 3 indicate the predominant atomic orbital contribution to each particular fragment molecular orbital. For clarity, the ligand-based orbitals are viewed in projection along the *z* axis; other orbitals are viewed perpendicular to this axis.

The highest occupied molecular orbital (HOMO) ($1a_1$ level) of the $Zr(\eta^8\text{-}C_8H_8)$ fragment is metal based (95% Zr character) and contains two electrons. The lower-energy orbitals ($1e_2$ and below) are predominantly ligand based. For example, the $1e_2$ and $1e_1$ levels contain only 33 and 6% Zr atomic orbital character respectively. Therefore, as anticipated from conventional bonding interpretations using the Hückel $4n + 2$ rule, the η^8-C_8H_8 ligand has as a *formal* 2− charge and there are two remaining metal-based electrons available for further bonding interactions of the $Zr(\eta^8\text{-}C_8H_8)$ fragment. The ligand-based orbitals are essentially unperturbed by further bonding interactions of the $Zr(\eta^8\text{-}C_8H_8)$ fragment.

The orbitals of puckered (fold angle 163°) C_{2v} C_8H_8 are shown on the right-hand side of Fig. 3. To assist further description we shall refer to the numbering scheme illustrated below where the projection of the Zr atom onto the C(1), C(2), C(3), C(7), C(8) plane is indicated by the symbol ⊗. The 'hinge' between the two planar five-carbon linkages [namely atoms

Table 5 Parameters used in the extended-Hückel calculations

Atom	Orbital	H_{ii}/eV	ζ_1
Zr	4d	−10.13	3.835*
	5s	−9.75	1.817
	5p	−6.16	1.776
C	2s	−20.45	1.625
	2p	−10.65	1.625
H	1s	−13.50	1.30

* $\zeta_2 = 1.505$, $c_1 = 0.6224$, $c_2 = 0.5782$, where c_1 and c_2 are the coefficients used in the double-ζ expansion.

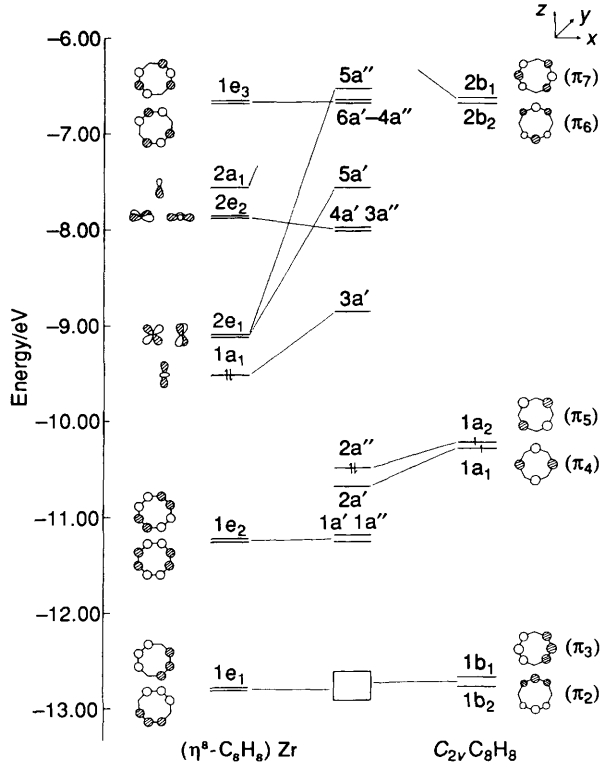

Fig. 3 Interaction diagram for $[Zr(\eta^8\text{-}C_8H_8)(\eta^3\text{-}C_8H_8)]$

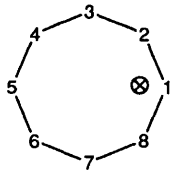

C(1), C(2), C(3), C(7), C(8) and C(3)–C(7)] is defined by the C(3)–C(7) vector. At the given fold angle of 163° the fragment orbitals of C_{2v} C_8H_8 are only relatively little perturbed (in energy and shape) from those of hypothetical planar (D_{8h}) C_8H_8.[7]

The level ordering shown at the centre of Fig. 3 for the whole complex has a satisfactory HOMO (2a″) – LUMO (lowest unoccupied molecular orbital) (3a′) gap indicative of a stable complex. The 3a′ level (LUMO) is predominantly metal-based (89% Zr character). The major contribution is from the Zr $4d_{z^2}$ atomic orbital (a little $4d_{xz}$ character is also mixed in as allowed by the low symmetry of this species) which, due to its particular nodal properties, has the poorest overlap with the frontier orbitals of the two C_8H_8 ligands. The HOMO (2a″) and SHOMO (second highest occupied molecular orbital) (2a′) are highly ligand based in nature (only 8 and 16% Zr contribution) and derive in the main part (82 and 71% respectively) from the η^3-C_8H_8 fragment orbitals indicated by the tie-lines in Fig. 3.

The metal-based $2e_1$ orbitals of the $Zr(\eta^8\text{-}C_8H_8)$ fragment have very similar computed overlaps with both the $1a_2$ and $1a_1$ and the $1b_2$ and $1b_1$ pairs of frontier orbitals of the η^3-C_8H_8 ligand. The 1a′ and 1a″ orbitals of the complex are formally derived from the $1e_2$ orbital pair of the $Zr(\eta^8\text{-}C_8H_8)$ fragment, retaining 85% of their fragment character (*i.e.* little mixing occurs with the η^3-C_8H_8 fragment orbitals).

We also considered the possibility of an interaction between the Zr atom and the C(3) and C(7) carbon atoms of the (formally) trihapto C_{2v} C_8H_8 ligand. The bond lengths between Zr and these atoms in the crystal structure of compound **2** are on average 2.84 Å, clearly long for a 'normal' π-type interaction but closer than anticipated for a simple non-bonding contact. When the calculations on our model complex were repeated with the overlap matrix elements between Zr and C(3) and C(7) set to zero we found a *stabilisation* of the 3a′ level (LUMO) of 0.5 eV, while the 2a′ level (SHOMO) was *destabilised* by 0.2 eV. So according to our calculations (and bearing in mind the approximations in our method and semiempirical choice of orbital basis set) there appears to be a significant degree of interaction between Zr and C(3) and C(7). Therefore, the hapticity of the puckered C_8H_8 moiety ought not to be considered as strictly three, but somewhere intermediate between three and five.

From an electron-counting standpoint the complex $[Zr(\eta^8\text{-}C_8H_8)(\eta^3\text{-}C_8H_8)]$ is best considered to possess two formally dianionic C_8H_8 ligands and contains Zr in a formal oxidation state of +4 (*i.e.* a d^0 complex using the standard nomenclature). That the η^3-C_8H_8 moiety formally acts as a dianionic ligand in the same way as a planar η^8-C_8H_8 ligand is not actually surprising given the very similar frontier orbitals of planar (D_{8h}) C_8H_8 and slightly puckered C_{2v} C_8H_8. If the 3a′ level (Fig. 3) is largely metal–ligand non-bonding then $[Zr(\eta^8\text{-}C_8H_8)(\eta^3\text{-}C_8H_8)]$ is a 16-valence-electron complex. However, if, as our numerical experiments with the Zr–C(3)/C(7) overlaps suggest, there is a significant degree of metal–ligand antibonding character in the 3a′ level, then some 18-valence-electron character is present (because all nine zirconium valence atomic orbitals are then involved in metal–ligand bonding).

We may also make a comparison with the anion $[Nb(\eta^4\text{-}C_8H_8)(\eta^3\text{-}C_8H_8)_2]^-$ in which one tetrahapto and two (formally) trihapto cyclooctatetraene ligands are present.[8] In this molecule (formally 16-valence-electron) the Nb–C distances to the next two carbon atoms of the η^3-C_8H_8 ligands average 3.13 Å [range 3.045(16)–3.217(14) Å]. On bond-length criteria alone, the importance of some pentahapto nature in the η^3-C_8H_8 ring–metal binding is somewhat less than in compound **2**.

We describe He I and He II photoelectron spectra for complex **2** in section (*ii*), but now turn to a consideration of the bonding in the closely related isomer $[Zr(\eta^8\text{-}C_8H_8)(\eta^4\text{-}C_8H_8)]$. The results of an EHMO calculation are shown in Fig. 4 in the form of an interaction diagram between a $Zr(\eta^8\text{-}C_8H_8)$ fragment and a C_s symmetry C_8H_8 fragment. In this case the model was based on the geometry of the real complex $[Zr(\eta^8\text{-}C_8H_8)(\eta^4\text{-}C_8H_8)]$, previously described by Floriani[3] and Girolami[9] and co-workers, and idealised to possess C_s symmetry. The atomic parameters used in the calculation are those listed in Table 5. Again in order to assist further description we shall refer to a numbering scheme (shown below) for the η^4-C_8H_8 ligand. The projection of the Zr atom onto the C(1), C(2), C(7), C(8) plane is indicated by the symbol ⊗.

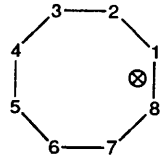

The η^4-C_8H_8 ligand thus binds to Zr through atoms C(1), C(2), C(7) and C(8) and the whole ring may be considered to

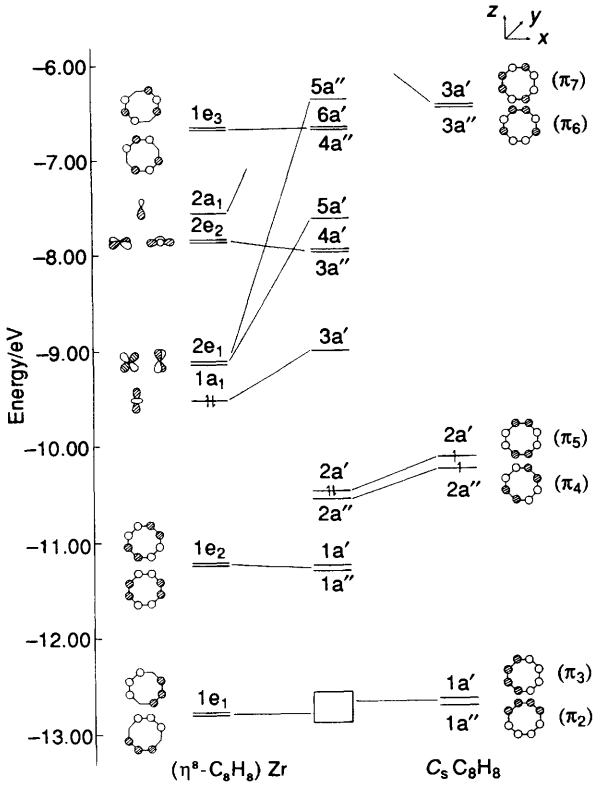

Fig. 4 Interaction diagram for $[Zr(\eta^8\text{-}C_8H_8)(\eta^4\text{-}C_8H_8)]$

consist of three planes [C(1), C(2), C(7), C(8); C(2), C(3), C(6), C(7); and C(3), C(4), C(5), C(6)]. The angle between the first two planes is 161° and that between the second and the third is 168° The 'hinges' between the pairs of planes are defined by the C(2)–C(7) and C(3)–C(6) vectors respectively. The η^4-C_8H_8 ligand thus possesses C_s symmetry. As with the orbitals of puckered C_{2v} C_8H_8 (on the right in Fig. 3), those of C_s C_8H_8 (on the right in Fig. 4) are closely related to those of planar (D_{8h}) C_8H_8 in energy and shape because the perturbation from the ideal (planar) geometry is not very substantial. The molecular-orbital diagram for the whole $[Zr(\eta^8\text{-}C_8H_8)(\eta^4\text{-}C_8H_8)]$ complex shown at the centre in Fig. 4 reveals a large HOMO – LUMO gap indicative of a stable geometry. The 3a' level (LUMO) is metal-based (89% Zr character) with the major contribution being from the $4d_{z^2}$ atomic orbital of Zr. The 2a' (HOMO) and 2a'' (SHOMO) levels are ligand based (15 and 8% Zr character) and predominantly localised on the η^4-C_8H_8 fragment.

The similarity of the computed molecular-orbital diagrams for the two isomers $[Zr(\eta^8\text{-}C_8H_8)(\eta^3\text{-}C_8H_8)]$ (Fig. 3) and $[Zr(\eta^8\text{-}C_8H_8)(\eta^4\text{-}C_8H_8)]$ (Fig. 4) is striking. The HOMO – LUMO gap for $[Zr(\eta^8\text{-}C_8H_8)(\eta^3\text{-}C_8H_8)]$ is somewhat larger by *ca.* 0.2 eV and is mainly due to a more substantial destabilisation of the $1a_1$ $Zr(\eta^8\text{-}C_8H_8)$ fragment molecular orbital in this isomer [consistent with our suggestion of a weak interaction between the Zr atom and the C(3) and C(7) carbon atoms of the η^3-C_8H_8 ligand]. The overall computed fragment charges [*i.e.* the degree of net electron gain on binding to the $Zr(\eta^8\text{-}C_8H_8)$ unit] for the η^3- and η^4-C_8H_8 ligands are virtually identical. Both rings in $[Zr(\eta^8\text{-}C_8H_8)(\eta^4\text{-}C_8H_8)]$ bear formal 2– charges and the Zr atom has a formal 4+ oxidation state. So similar are the two complexes that there is virtually no difference in the total energies (*i.e.* sum of the one-electron energies) for the two models with the geometries used. We cannot, from our calculations, account for the choice of one isomer over the other on orbital preferences alone (compare the differing structures of $[Zr\{\eta^8\text{-}C_8H_6(SiMe_3)_2\}\{\eta^3\text{-}C_8H_6(SiMe_3)_2\}]$ and $[Hf\{\eta^8\text{-}C_8H_6(SiMe_3)_2\}\{\eta^4\text{-}C_8H_6(SiMe_3)_2\}]$). Guggenberger and Schrock[8] have pointed out that for cyclooctatetraene ligands 'a near continuum of closely related conformations is possible especially where packing forces might stabilise lower symmetry conformations'.

As a final point of interest we repeated our calculation for $[Zr(\eta^8\text{-}C_8H_8)(\eta^4\text{-}C_8H_8)]$ but this time set all the C–C distances in the η^4-C_8H_8 ligand to be equal (1.41 Å) in order to compare Mulliken overlap populations between these carbon atoms. The level ordering and relative energies in this model were virtually indistinguishable from those shown in Fig. 4. The computed net C–C overlap populations are illustrated below [the projection of the Zr atom onto the C(1), C(2), C(7), C(8) plane is again indicated by the symbol ⊗].

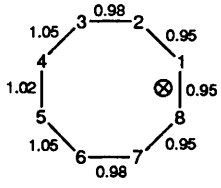

At constant C–C bond lengths a larger Mulliken overlap population between two atoms signals a likelihood for the bond to shorten in the real complex. The sequence of overlap populations suggests that the four non-metal-bound carbon atoms [*i.e.* C(3)–C(6)] should show alternating short–long–short bond lengths while the bond lengths between the carbons bound to the metal [*i.e.* C(1), C(2), C(7), C(8)] should be very similar and supports the proposals of previous workers.[10] This type of bond-length sequence has been found crystallographically in some complexes containing a η^4-C_8H_8 ligand,[10,11] although others do not show any clear sequence (possibly due to lack of precision in the X-ray analysis), including $[Zr(\eta^8\text{-}C_8H_8)(\eta^4\text{-}C_8H_8)]$.[3,9,12] We have also carried out a separate calculation on the C_s C_8H_8 fragment of Fig. 4 alone with a formal 2– charge and equal C–C bond lengths; this time there was no such significant variation in C–C overlap populations around the ring. Therefore the variations we see in overlap populations for the tetrahapto cyclooctatetraene ligand when bound to metal appear to be a real consequence of orbital interaction, rather than of simple transfer of electron density and/or geometrical perturbation.

(ii) Gas-phase UV Photoelectron (PE) Spectra of $[Zr\{\eta^8\text{-}C_8H_6(SiMe_3)_2\}\{\eta^3\text{-}C_8H_6(SiMe_3)_2\}]$.—The He I and He II PE spectra of $[Zr\{\eta^8\text{-}C_8H_6(SiMe_3)_2\}\{\eta^3\text{-}C_8H_6(SiMe_3)_2\}]$ have been measured (Fig. 5). Table 6 gives ionisation energies, assignments and $R_{II/I}$ values (relative areas in the He II spectrum divided by those in the He I) for the bands labelled A–E in Fig. 5.

Above *ca.* 9.5 eV two broad bands (D and E) may be distinguished. The profile and ionisation energies of these bands are extremely similar to those of corresponding peaks in the PE spectra of $[U\{\eta^8\text{-}C_8H_6(SiMe_3)_2\}_2]$[13] and $[U\{\eta^8\text{-}C_8H_7(SiMe_3)\}_2]$,[14] and closely resemble those of the free cyclooctatetraene.[13] The large number of orbitals ionising in this region makes detailed assignment impossible but, in agreement with previous workers,[13,14] we propose that band D may be identified with Si–C σ-bonding orbitals and E with C–C and C–H σ MOs. The most stable ring π ionisations will also lie under these bands. None of the MOs giving rise to bands D and E is responsible for binding the ligands to the metal, and these bands will not be discussed further.

There are three bands ionising between 5.5 and 9.5 eV, the first of which (A) displays a marked asymmetry under higher resolution [Fig. 5(b)]. The latter is ascribed to the 2a' and 2a'' MOs (Fig. 3), with band B being assigned to the 1a' and 1a'' and band C to the MOs derived from the $1e_1$ levels of the $[Zr\{\eta^8\text{-}C_8H_6(SiMe_3)_2\}]$ fragment together with π_2 and π_3 of the η^3-$C_8H_6(SiMe_3)_2$ unit.

Table 6 Ionisation energies, band assignments and $R_{II/I}$ values in the PE spectrum of $[Zr\{\eta^8\text{-}C_8H_6(SiMe_3)_2\}\{\eta^3\text{-}C_8H_6(SiMe_3)_2\}]$

Band	Ionisation energy/eV	Assignment	$R_{II/I}$
A (adiabatic)	5.54		
A (vertical)	6.18	2a′, 2a″	1.00
A′	6.58		
B	7.69	1a′, 1a″	1.14
C	8.95	$[Zr\{\eta^8\text{-}C_8H_6(SiMe_3)_2\}]$ $1e_1$ + $\eta^3\text{-}C_8H_6(SiMe_3)_2$ π_2 and π_3	0.471
D	10.45	Si–C σ bonding	
E	13.20	C–C, C–H σ bonding	

The $R_{II/I}$ values indicate that band B gains in intensity relative to the other bands as the photon energy is increased from He I to He II. This is consistent with the results of the calculation, in which the 1a′ and 1a″ MOs are computed to have a greater metal d-orbital contribution than have any other MO. The well established gain in relative intensity of d-orbital-based MOs with respect to hydrocarbon ligand MOs as the ionising radiation is changed from He I to He II arises principally as a result of the greater rate of fall off in photoionisation cross-section of carbon 2p and hydrogen 1s AOs with respect to metal d orbitals.[15]

It is instructive to compare the ionisation energies of bands A and B with those of corresponding bands in the PE spectrum of $[U\{\eta^8\text{-}C_8H_6(SiMe_3)_2\}_2]$.[13] As indicated in the discussion of the EHMO calculations, the puckering of a $C_8H_6(SiMe_3)_2$ ring does not represent a major perturbation to the MOs of a planar D_{8h} system, and band A may be equated with the valence e_{2u} MOs of $[U\{\eta^8\text{-}C_8H_6(SiMe_3)_2\}_2]$ and B with the e_{2g} set (the first band in the PE spectrum of $[U\{\eta^8\text{-}C_8H_6(SiMe_3)_2\}_2]$ arises, of course, from ionisation of the two f electrons). The e_{2g} MOs may have a metal d-orbital contribution but no f-orbital character, the opposite being true for the e_{2u} set.

The ionisation energies of band B of $[Zr\{\eta^8\text{-}C_8H_6(SiMe_3)_2\}\{\eta^3\text{-}C_8H_6(SiMe_3)_2\}]$ and the e_{2g} band of $[U\{\eta^8\text{-}C_8H_6(SiMe_3)_2\}_2]$ are very similar, 7.69 and 7.53 eV respectively. Both levels are stabilised by interaction with the metal d orbitals. In contrast, the energies of band A and the e_{2u} levels of $[U\{\eta^8\text{-}C_8H_6(SiMe_3)_2\}_2]$ are less coincident, at 6.18 and 6.65 eV. The e_{2u} MOs of $[U\{\eta^8\text{-}C_8H_6(SiMe_3)_2\}_2]$ are stabilised by a contribution from the metal f orbitals, an interaction which is not present in the zirconium complex. While the lowering of symmetry between $[U\{\eta^8\text{-}C_8H_6(SiMe_3)_2\}_2]$ and $[Zr\{\eta^8\text{-}C_8H_6(SiMe_3)_2\}\{\eta^3\text{-}C_8H_6(SiMe_3)_2\}]$ permits some metal d-orbital admixture to the 2a′ and 2a″ MOs, it is clearly not as great a stabilising effect as the metal f-orbital contribution in the uranium complex.

As discussed in the section on the EHMO calculations, there are only very small energy differences between $[Zr\{\eta^8\text{-}C_8H_6(SiMe_3)_2\}\{\eta^3\text{-}C_8H_6(SiMe_3)_2\}]$ and $[Zr\{\eta^8\text{-}C_8H_6(SiMe_3)_2\}\{\eta^4\text{-}C_8H_6(SiMe_3)_2\}]$. Thus while $[Zr\{\eta^8\text{-}C_8H_6(SiMe_3)_2\}\{\eta^3\text{-}C_8H_6(SiMe_3)_2\}]$ is present in the solid state, it must be noted that the gas-phase species may not be the same. It is not possible to tell from the PE data whether the η^3 mode is preserved in the gas phase, or whether a change to η^4 co-ordination occurs. The calculations indicate that the electronic structures of the two systems are almost identical and hence would be expected to give rise to similar PE spectra. The gap between the 2a′ and 2a″ MOs is calculated as being greater in the η^3 complex, which may explain the asymmetry of band A, but no definite conclusions can be drawn from the PE spectra.

Conclusions

The results on $[M\{C_8H_6(SiMe_3)_2\}_2]$ (M = Ti or Zr) presented herein, in conjunction with the previously reported work on the hafnium analogue by Floriani and co-workers,[3] complete the series and allow comparisons to be made with the unsubstituted analogues $[M(C_8H_8)_2]$ (M = Ti or Zr). We conclude that there is little energetic preference for η^4- *vs.* η^3-bound $C_8H_6(SiMe_3)_2$, as indicated by the calculations and PE studies, and adoption of a particular solid-state structure is essentially determined by the steric requirements of the $SiMe_3$ substituents. Thus in the $[M(C_8H_8)_2]$ compounds, where the latter feature is absent, pure η^4 co-ordination is observed. In solution, however, the relative sizes of Ti *vs.* Zr are probably equally important in determining the rate of ring interconversion since both $[Ti(C_8H_8)_2]$ and $[Ti\{C_8H_6(SiMe_3)_2\}_2]$ are static on the NMR time-scale at room temperature whereas both zirconium analogues are fluxional down to 173 K. Indeed, the solid-state structure of $[Zr\{C_8H_6(SiMe_3)_2\}_2]$ may represent the transition state *via* which ring interconversion proceeds in $[Ti\{C_8H_6(SiMe_3)_2\}_2]$, in an analogous manner to that proposed for the compounds $[M(C_5H_5)_4]$ (M = Ti or Zr).[16]

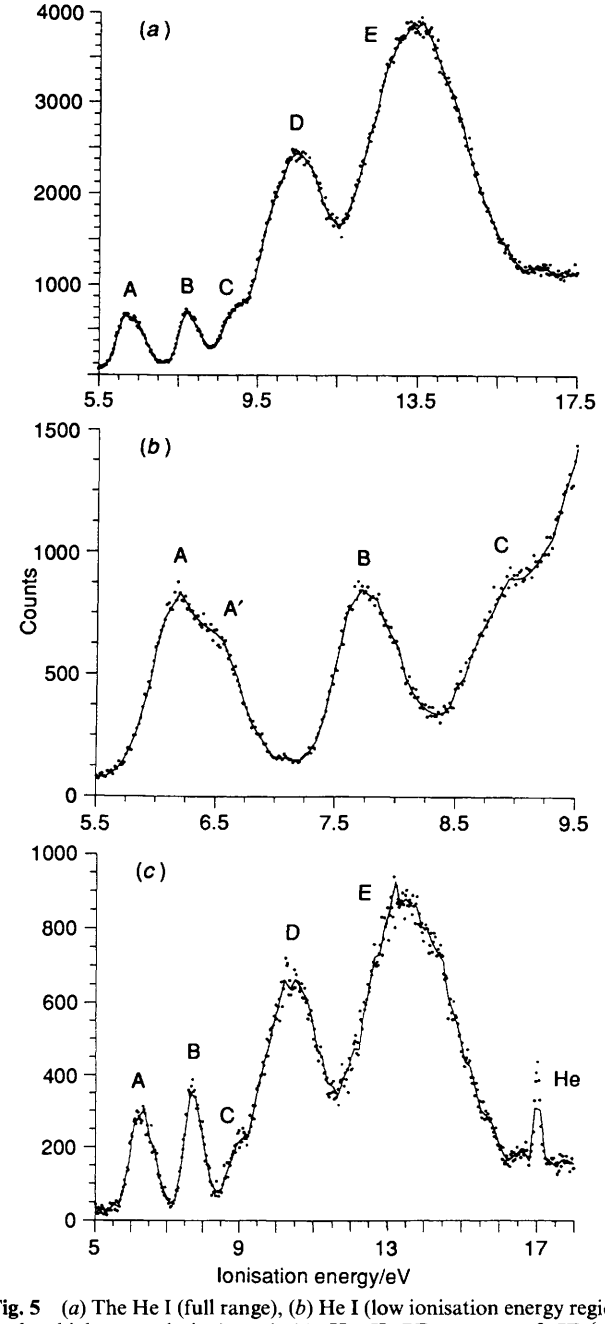

Fig. 5 (*a*) The He I (full range), (*b*) He I (low ionisation energy region under higher resolution) and (*c*) He II PE spectra of $[Zr\{\eta^8\text{-}C_8H_6(SiMe_3)_2\}\{\eta^3\text{-}C_8H_6(SiMe_3)_2\}]$

Experimental

General Procedures and Techniques.—All manipulations (unless otherwise stated) were conducted in an inert atmosphere of argon or dinitrogen. This was achieved using conventional Schlenk-line techniques under an argon atmosphere, or in a Miller–Howe or Braun glove-box under an atmosphere of dinitrogen (< 5 ppm H_2O, < 1 ppm O_2). The synthesis of the lithium reagent $[Li_2\{C_8H_6(SiMe_3)_2\}]$ has been described previously[2] and the thf-solvated adducts of zirconium and titanium were prepared by published procedures.[17] All solvents were pre-dried by distillation under dinitrogen over the appropriate drying agent [toluene (sodium), light petroleum (b.p. 40–60 °C) and pentane (sodium–potassium alloy), thf (potassium)], degassed and stored over a potassium mirror under argon in glass ampoules equipped with Rotaflo stopcocks.

All glassware, cannulae and Celite were stored in an oven (> 373 K) and glassware and Celite were flame-dried *in vacuo* immediately prior to use. Unless otherwise stated, all other reagents and chemicals were obtained from the Aldrich Chemical Co. and used without further purification. Deuteriated solvents were from M.S.D. Isotopes; prior to use, they were degassed by the freeze–thaw method, refluxed over molten potassium, and vacuum transferred into a glass ampoule fitted with a Youngs tap and stored in the glove-box.

The PE spectra were measured using a PES Laboratories 0078 spectrometer interfaced with an Atari 1040 ST microcomputer. Both He I and He II radiation were used for spectral acquisition. Data were collected by repeated scans and the spectra calibrated with He, Xe and N_2. Band areas were obtained by fitting with asymmetric Gaussian curves and were normalised to those of the first band. In spectral plots the dots represent the data points and the continuous line a weighted smoothing of the data.

Solution NMR spectra were recorded on Bruker ACP250, WM360 or AMX500 instruments at ambient temperature unless otherwise stated. Chemical shifts (δ) are relative to the residual proton chemical shift of the deuteriated solvent (^1H), the carbon chemical shift of the deuteriated solvent (^{13}C), or external tetramethylsilane (^{29}Si). Solid-state ^{29}Si NMR spectra were recorded on a Bruker ACP250 instrument and referenced to external Q8M8 [$(Me_3SiOSiO_3)_8$] (Dow Corning).

Electron impact (EI) mass spectra were recorded on a Kratos MS80RF instrument. Microanalyses were performed by Medac Ltd. or Canadian Microanalytical Services Ltd.

$[Ti\{C_8H_6(SiMe_3)_2\}_2]$ **1**.—To a thf (30 cm^3) solution of $[TiCl_4(thf)_2]$ (0.20 g, 0.6 mmol) at 0 °C was added a thf (30 cm^3) solution of $[Li_2\{C_8H_6(SiMe_3)_2\}]$ (0.417 g, 1.32 mmol) dropwise over 40 min. Initially no change in colour was observed, however after about one half of the ligand solution had been added a pale green colour was evident. This soon darkened to afford a red brown solution which was allowed to stir at room temperature overnight. The solvent was removed *in vacuo* to afford a red oil, which was redissolved in light petroleum and filtered through Celite to afford a red solution. The latter was concentrated to dryness to afford compound **1**, again as a red oil. The oil was redissolved in pentane, the solution concentrated to *ca.* 20 cm^3 and placed in a freezer at −30 °C. After 2 weeks a microcrystalline solid had been formed; sublimation [125 °C, 10^{-6} mmHg (*ca.* 1.33 × 10^{-4} Pa)] afforded large translucent dark red crystals of pure **1**. Yield 0.17 g, 52% (Found: C, 61.70; H, 8.75. $C_{28}H_{48}Si_4Ti$ requires C, 61.70; H, 8.85%). NMR ($C_6D_5CD_3$): ^1H, δ 6.91 (2 H, m, CH of ring), 6.61 (2 H, s, CH of ring), 6.58 (2 H, s, CH of ring), 6.36 (2 H, m, CH of ring), 6.11 (2 H, s, CH of ring), 5.92 (2 H, m, CH of ring), 0.50 (18 H, s, $SiMe_3$), and 0.31 (18 H, s, $SiMe_3$); ^{13}C-{^1H}, δ 121.2 (s, C–$SiMe_3$ of ring), 114.5 (s, CH of ring), 112.6 (s, CH of ring), 112.3 (s, CH of ring), 108.1 (s, CH of ring), 104.0 (s, CH of ring), 102.4 (s, CH of ring), 100.4 (s, C–$SiMe_3$ of ring), 0.74 (s, 2 $SiMe_3$), and 0.17 (s, 2 $SiMe_3$); ^{29}Si-{^1H}, δ 10.33 (s, 2 $SiMe_3$) and 0.23 (s, 2 $SiMe_3$). Mass spectrum (EI): *m/z* 544 (8, M^+), 471 (7, $M - SiMe_3$), 296 [100, $M - C_8H_6(SiMe_3)_2$], 249 [9, $M - Ti[C_8H_8(SiMe_3)_2]$-(+1)], and 73 (74%, $SiMe_3$).

Structure determination. Crystal data. $C_{28}H_{48}Si_4Ti$, M = 588.9, orthorhombic, space group $Pca2_1$, a = 14.199(9), b = 11.716(8), c = 18.863(12) Å, U = 3138.0 Å^3, λ(Mo-Kα) = 0.710 73 Å, Z = 4, D_c = 1.153 g cm^{-3}, $F(000)$ = 1176, μ = 0.44 mm^{-1}, R = 0.0538, R' = 0.0666 for 1901 observed reflections [$|F^2| \geqslant 4\sigma(F^2)$] with $W = 1/[\sigma^2(F) + 0.003F^2]$. Dark red, air-sensitive blocks. Crystal dimensions 0.45 × 0.20 × 0.23 mm.

The crystal was mounted in a Lindeman capillary under argon and held at 240 K with an Oxford Cryosystems Cryostream Cooler (Cosier and Glazer 1986) on a Siemens R3m diffractometer. Scan speed 3–15°(ω) min^{-1}, depending on the intensity of a 2 s pre-scan; backgrounds were measured at each end of the scan for 0.25 of the scan time. The data were rescaled to correct for crystal decay (3%). Reflections were processed using profile analysis. No absorption correction was applied. The structure was solved by direct methods using SHELXTL (TREF)[18] and the light atoms then found by E-map expansion and successive Fourier syntheses. Anisotropic thermal parameters were used for all non-H atoms. Hydrogen atoms were given fixed isotropic thermal parameters, U = 0.08 Å^2. Those defined by the molecular geometry were inserted at calculated positions and not refined; methyl groups were treated as rigid units, with their initial orientation based on a staggered configuration. The absolute structure of the individual crystal chosen was checked by refinement of the Flack parameter. Computing was with the SHELXTL PLUS program on a DEC MicroVax-II computer.

$[Zr\{C_8H_6(SiMe_3)_2\}_2]$ **2**.—To a colourless thf (30 cm^3) solution of $[ZrCl_4(thf)_2]$ (0.57 g, 1.5 mmol) at 0 °C was added a thf (30 cm^3) solution of $[Li_2\{C_8H_6(SiMe_3)_2\}]$ (1.0 g, 3.2 mmol) dropwise over 1 h. After complete addition the purple solution was allowed to stir at room temperature overnight. The solvent was removed *in vacuo* to afford a purple oil, subsequently redissolved in light petroleum and filtered through Celite to remove LiCl. The filtrates were concentrated and placed in a freezer at −30 °C for 3 d to afford the product **2** as purple crystals. Yield 0.53 g, 58% (Found: C, 56.10; H, 8.45. $C_{28}H_{48}Si_4Zr$ requires C, 57.15; H, 8.20%). NMR ($C_6D_5CD_3$): ^1H, δ 6.35 (2 H, s, CH of ring), 6.32 (2 H, m, CH of ring), 5.85 (2 H, m, CH of ring), and 0.35 (18 H, s, $SiMe_3$); ^{13}C-{^1H}, δ 109.9 (s, C–$SiMe_3$ of ring), 105.2 (s, CH of ring), 103.6 (s, CH of ring), 102.8 (s, CH of ring), and 0.5 (s, 2 $SiMe_3$); CP MAS ^{29}Si-{^1H}; δ 11.71 (s, $SiMe_3$), 9.67 (s, $SiMe_3$), 1.17 (s, $SiMe_3$), and −2.13 (s, $SiMe_3$); ^{29}Si-{^1H}; δ 6.63 (s, $SiMe_3$). Mass spectrum (EI): *m/z* 586 (14, M^+), 513 (11, $M - SiMe_3$), 338 [15, $M - C_8H_6(SiMe_3)_2$], 248 {6, $M - Zr[C_8H_6(SiMe_3)_2]$} and 73 (100%, $SiMe_3$).

Structure determination. Crystal data. $C_{28}H_{48}Si_4Zr$, M = 588.3, tetragonal, space group $I4_1/a$ (no. 88), $a = b$ = 29.540(5), c = 14.950(2) Å, U = 13 044.7 Å^3, λ(Mo-Kα) = 0.710 73 Å, Z = 16, D_c = 1.20 g cm^{-3}, $F(000)$ = 4992, μ = 0.49 mm^{-1}. Dark purple, air-sensitive crystals.

Data were collected on an Enraf–Nonius CAD4 diffractometer in the θ–2θ mode, using a crystal of dimensions *ca.* 0.4 × 0.4 × 0.15 mm mounted in a Lindeman capillary under argon. A total of 5965 unique reflections were measured for 2 < θ < 25° and $+h$, $+k$, $+l$, and 2183 reflections with $|F^2| > 2\sigma(F^2)$ were used in the refinement where $\sigma(F^2) = [\sigma^2(I) + (0.04I)^2]^{\frac{1}{2}}/L_p$ (L_p = Lorentz polarisation). A correction (maximum 1.19, minimum 0.76) was applied for absorption using DIFABS[19] after isotopic refinement. No decay correction was applied.

The structure was solved *via* heavy-atom methods using SHELXS 86[20] with non-H atoms refined anisotropically by full-matrix least squares. Methyl carbon atoms on Si(4) were disordered. Hydrogen atoms were held at fixed calculated positions with $U_{iso} = 1.3U_{eq}$ for the parent atom except for

those on disordered methyls which were omitted. With a weighting scheme of $w = 1/\sigma^2(F)$ the final residuals were $R = 0.051$ and $R' = 0.054$ with a ratio of observations to variables of 6.72:1, and $S = 1.3$.

Additional material available for both structures from the Cambridge Crystallographic Data Centre comprises H-atom coordinates, thermal parameters and remaining bond lengths and angles.

Acknowledgements

We thank the SERC and BP (Dr. J. P. McNally) for support of this work.

References

1 N. C. Burton, F. G. N. Cloke, P. B. Hitchcock, H. C. de Lemos and A. A. Sameh, *J. Chem. Soc., Chem. Commun.*, 1989, 1462.
2 N. C. Burton, F. G. N. Cloke, S. C. P. Joseph, H. Karamallakis and A. A. Sameh, *J. Organomet. Chem.*, 1993, **462**, 39.
3 P. Berno, C. Floriani, A. Chiesi-Villa and C. Rizzoli, *J. Chem. Soc., Dalton Trans.*, 1991, 3085.
4 J. Schwartz and J. E. Sadler, *J. Chem. Soc., Chem. Commun.*, 1973, 172.
5 H. Dietrich and M. Soltwisch, *Angew. Chem., Int. Ed. Engl.*, 1969, **8**, 765.
6 R. Hoffmann and W. N. Lipscomb, *J. Chem. Phys.*, 1962, **36**, 2179.
7 F. A. Cotton, *Chemical Applications of Group Theory*, 3rd edn., Wiley, New York, 1990.
8 L. J. Guggenberger and R. R. Schrock, *J. Am. Chem. Soc.*, 1975, **97**, 6693.
9 D. M. Rogers, S. R. Wilson and G. S. Girolami, *Organometallics*, 1991, **10**, 2419.
10 B. Dickens and W. N. Lipscomb, *J. Chem. Phys.*, 1962, **37**, 2084; F. A. Cotton and R. Eiss, *J. Am. Chem. Soc.*, 1969, **91**, 6593.
11 W. J. Highcock, R. M. Mills, J. L. Spencer and P. Woodward, *J. Chem. Soc., Dalton Trans.*, 1986, 831.
12 D. J. Brauer and C. Krüger, *J. Organomet. Chem.*, 1972, **42**, 129.
13 C. M. Redfern and J. C. Green, unpublished work.
14 G. Bruno, E. Ciliberto, R. D. Fischer, I. Fragala and A. W. Spieg, *Organometallics*, 1982, **1**, 1060.
15 J. C. Green, *Struct. Bonding (Berlin)*, 1981, **43**, 37.
16 J. L. Calderon, F. A. Cotton and J. Takats, *J. Am. Chem. Soc.*, 1971, **93**, 3587; J. L. Calderon, F. A. Cotton, J. Takats and B. G. de Boer, *J. Am. Chem. Soc.*, 1971, **93**, 3592.
17 L. E. Manzer, *Inorg. Synth.*, 1981, **21**, 135.
18 G. M. Sheldrick, SHELXTL PLUS, Siemens Analytical Instruments, Madison, WI, 1990.
19 N. Walker and D. Stuart, *Acta Crystallogr., Sect. A*, 1983, **39**, 158.
20 G. M. Sheldrick, SHELXS 86, University of Göttingen, 1986.

Received 4*th May* 1994; *Paper* 4/02640C